Science Advances
AAAS

Supplementary Materials for

Rapid liquid phase–assisted ultrahigh-temperature sintering of high-entropy ceramic composites

Hua Xie *et al.*

Corresponding author: Liangbing Hu, binghu@umd.edu; Jian Luo, jluo@alum.mit.edu

Sci. Adv. **8**, eabn8241 (2022)
DOI: 10.1126/sciadv.abn8241

This PDF file includes:

Figs. S1 to S13

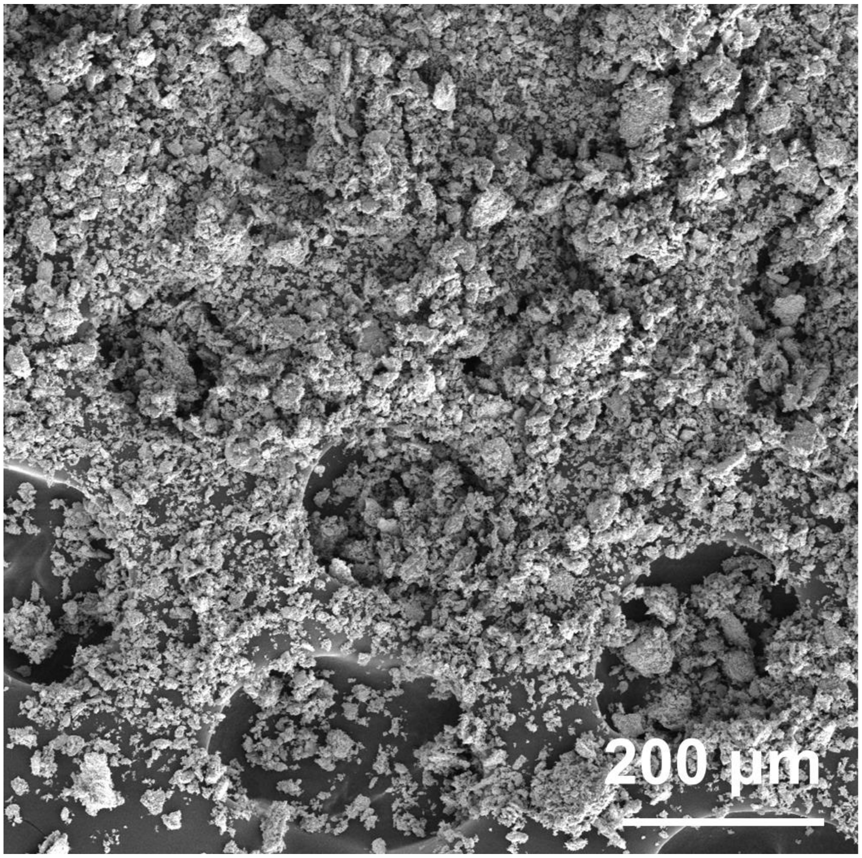

Fig. S1. The milled HEB/boron carbide powders after the self-propagating reaction.

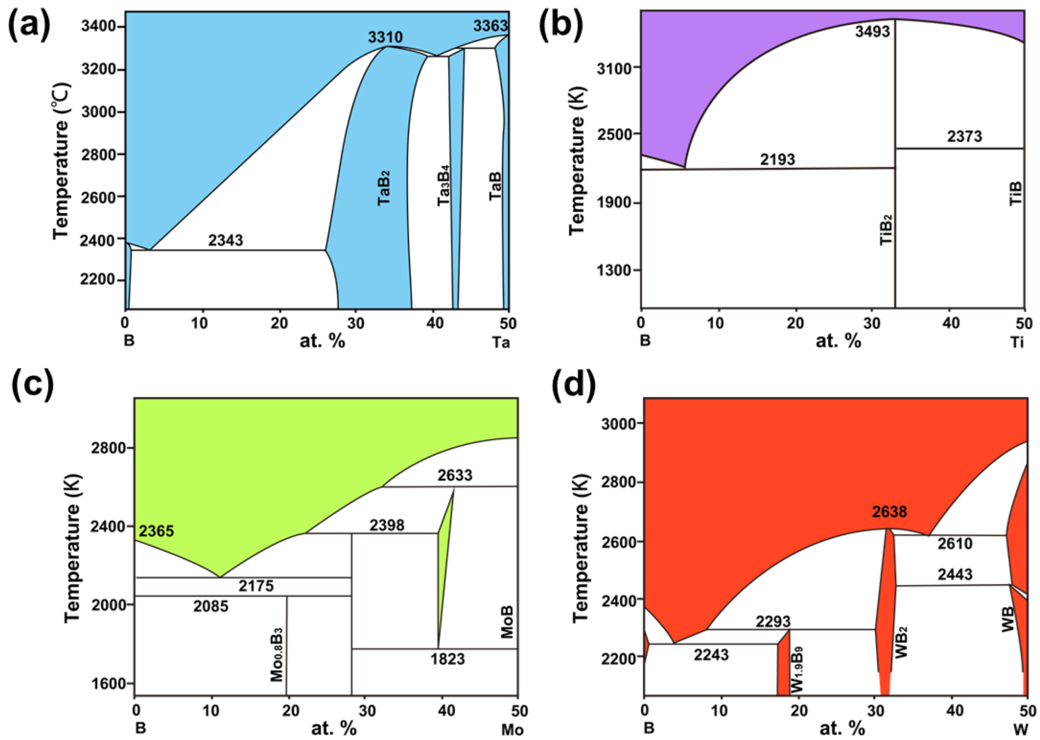

Fig. S2. Phase diagrams between boron and various transition metals. (a) Ta-B, (b) Ti-B, (c) Mo-B, and (d) W-B, respectively. The 3,000 K sintering temperature can maintain the HEB in a solid state *(38-40)*.

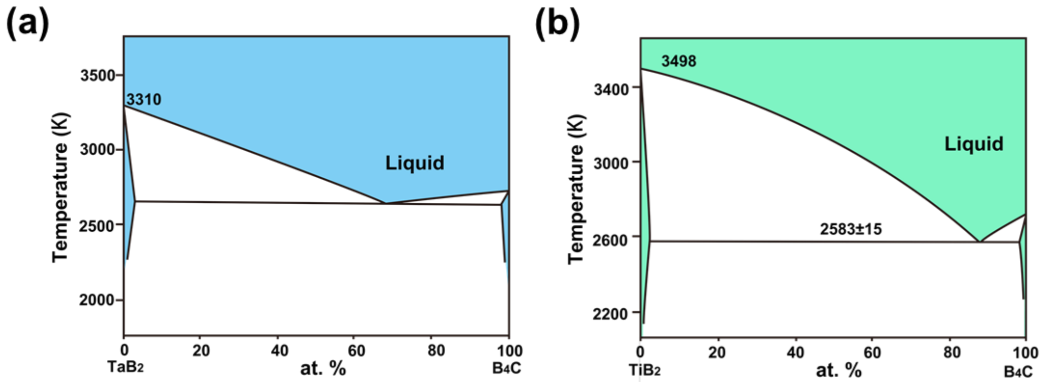

Fig. S3. Phase diagrams between boron carbide and diborides. (a)TaB_2 and (b) TiB_2 The eutectic liquid presents a pronounced melting point drop, which facilitates the formation of the intergranular phase *(38-40)*.

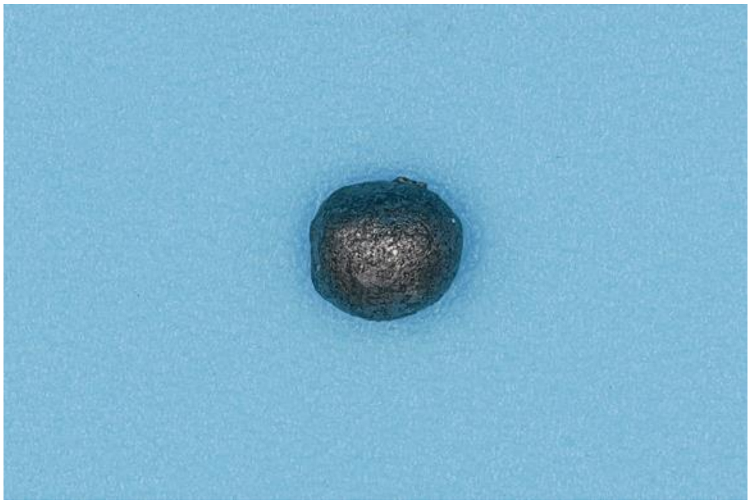

Fig. S4. Sample morphology. The HEB composite melts, loses its original geometry and becomes a spherical ingot, when the heating treatment temperature is ~3300 K.

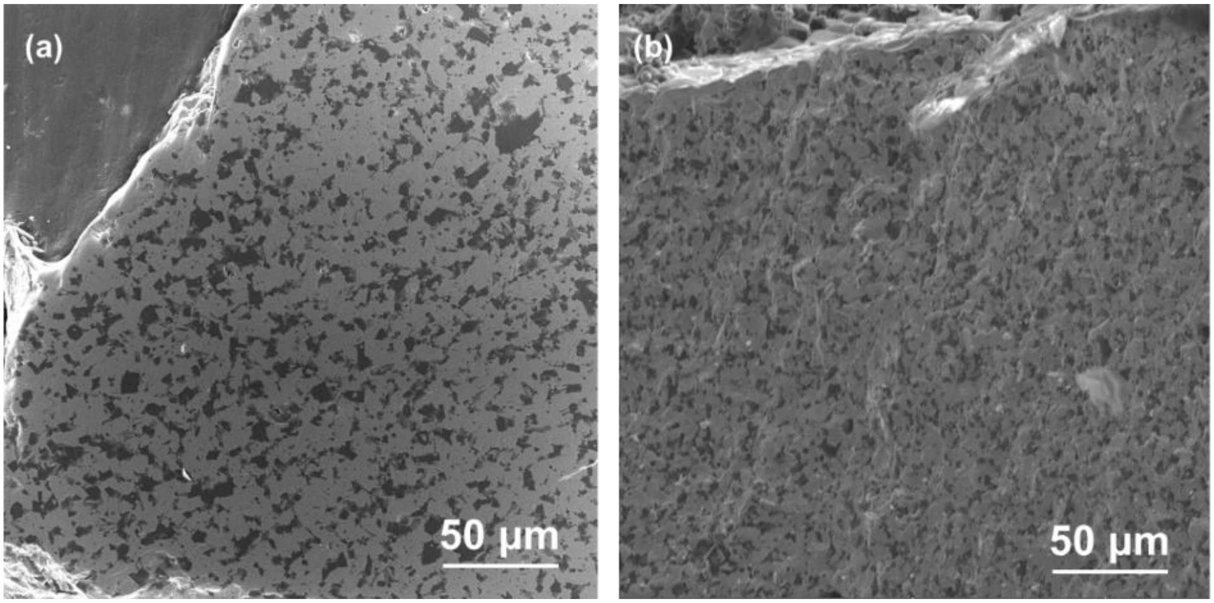

Fig. S5. Cross-sectional SEM images of the HEB composite. (a) Polished and (b) fractured.

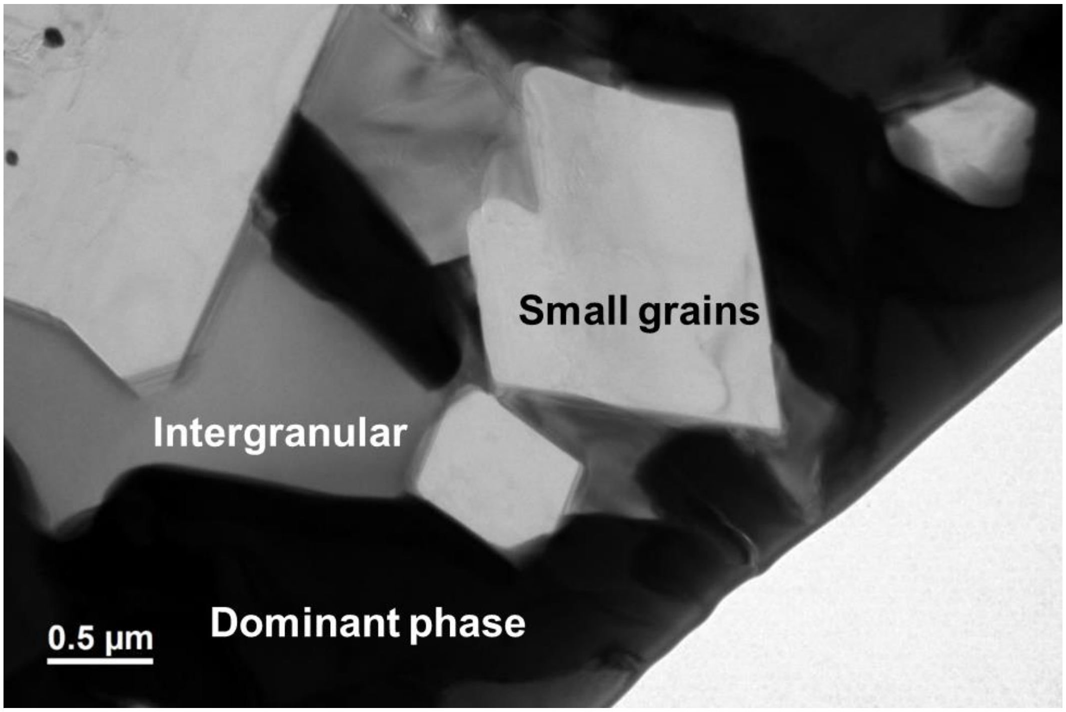

Fig. S6. TEM image of the HEB composite ceramic prepared via a focused ion beam. Three different phases can be differentiated: the dominant phase, the small grains, and the intergranular phase.

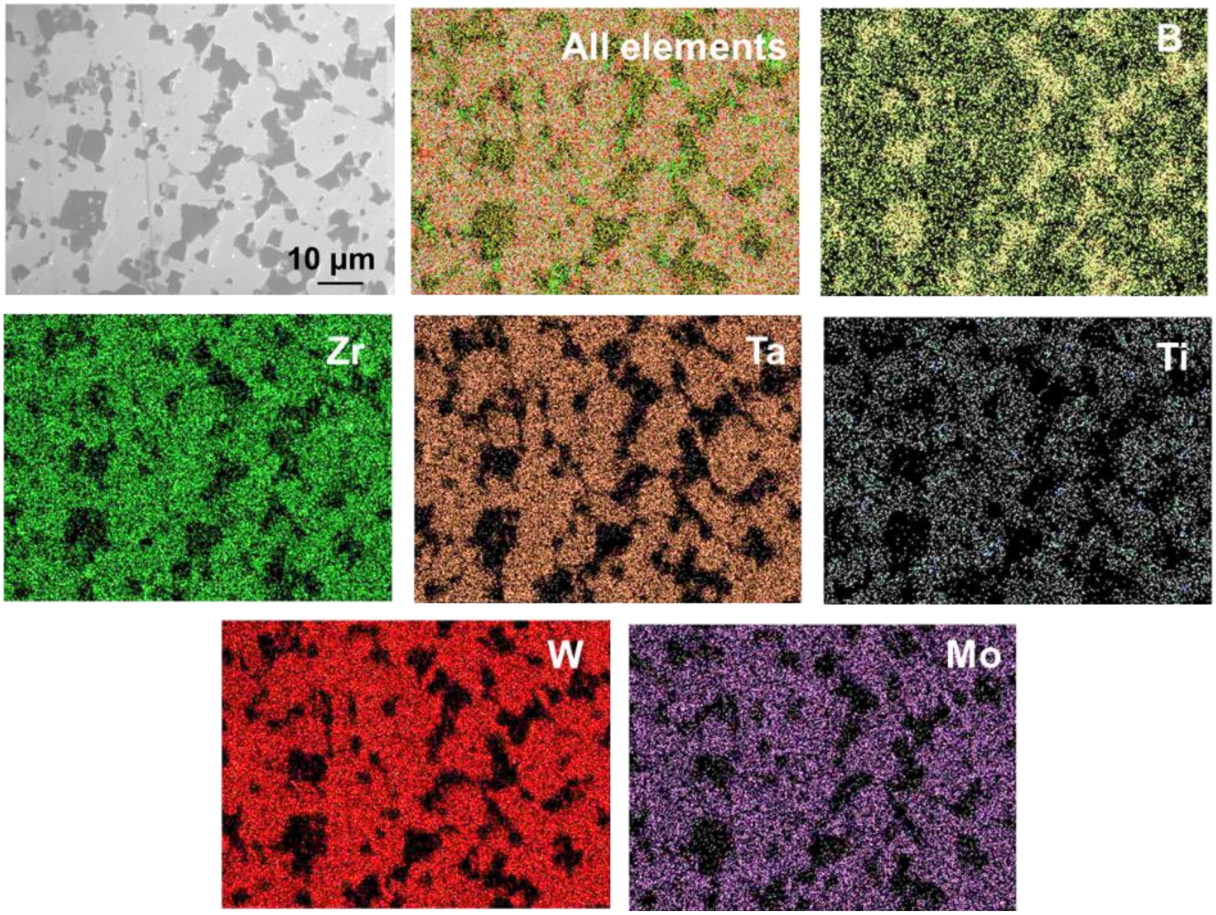

Fig. S7. SEM EDS mapping of the HEB composite ceramic. The metal elements are uniformly distributed in the HEB phase.

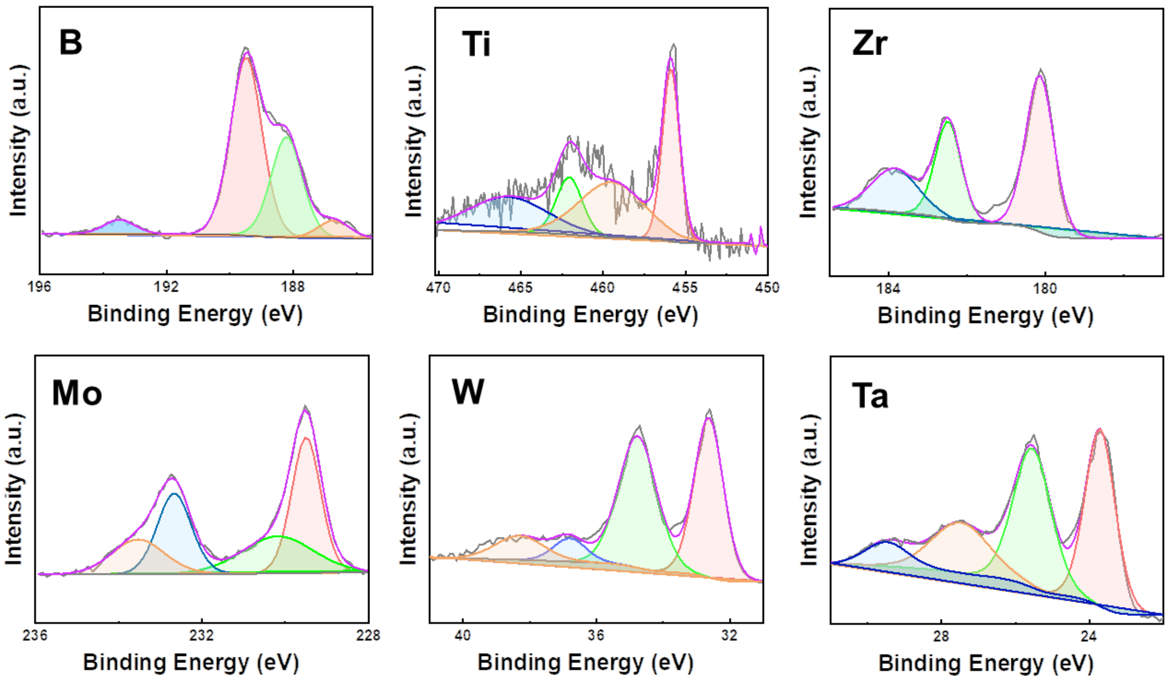

Fig. S8. XPS spectra of the different elements in the synthesized HEB and boron carbide composite ceramic. The boron element presents multiple valence states, which is consistent with the EELS analysis we achieved in Fig. 4.

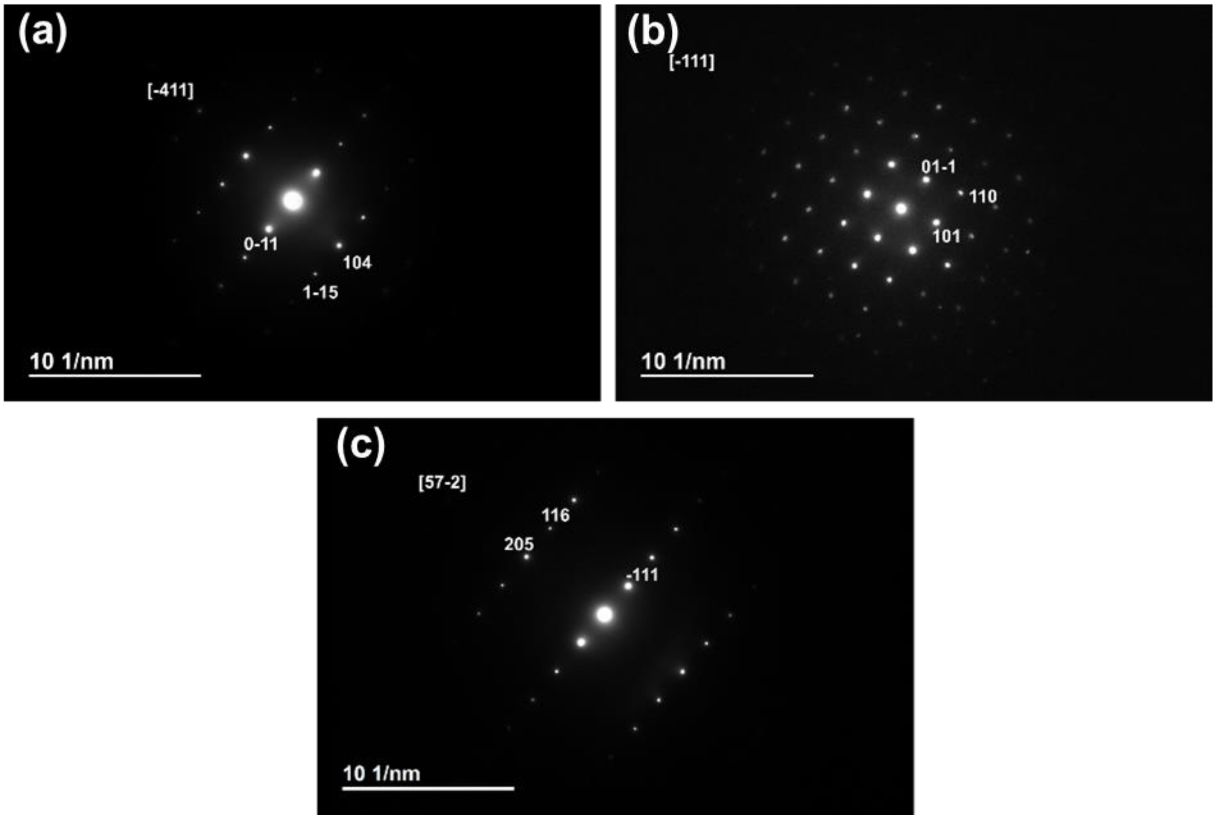

Fig. S9. Electron diffraction pattens for $B_{13}C_2$. Taken along the zone axes of (a) [-411], (b) [-111], and (c) [57-2], respectively.

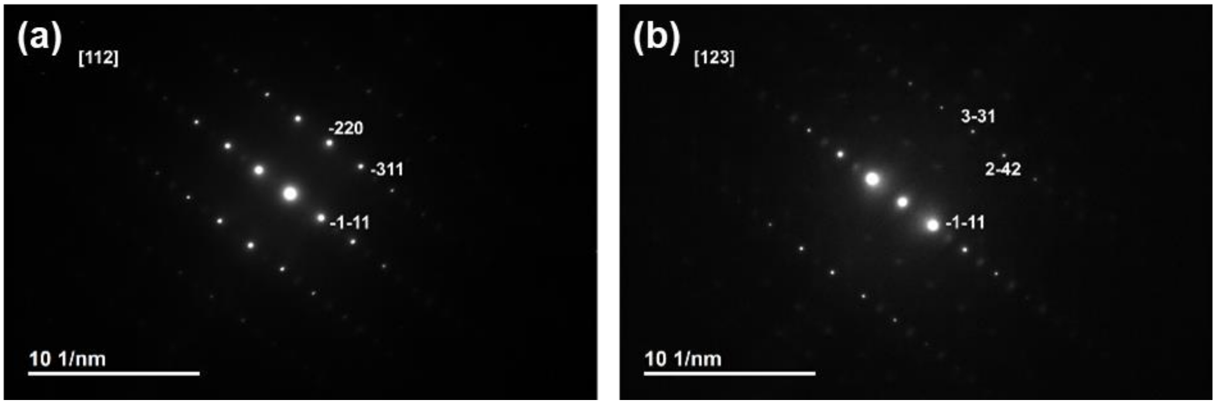

Fig. S10. Electron diffraction pattens for ZrB_{12}. Taken along the zone axes of (a) [112] and (b) [123].

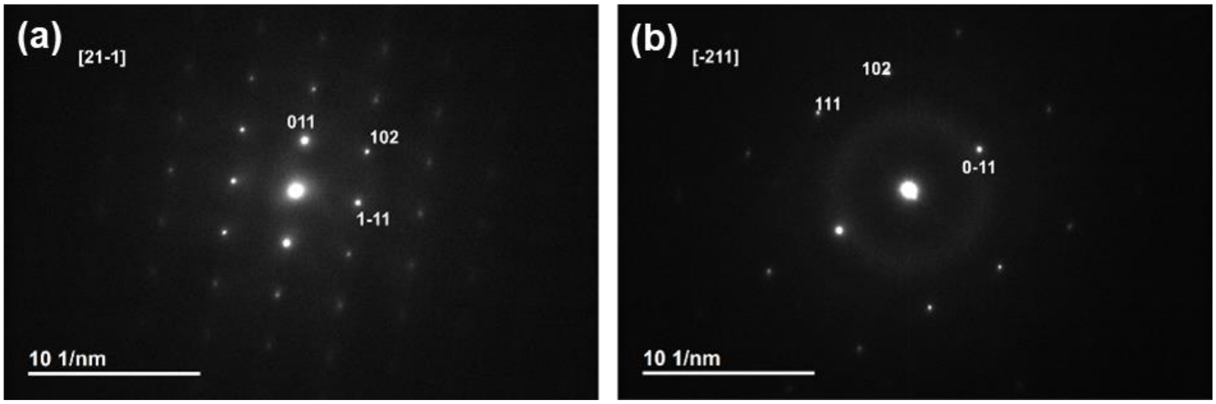

Fig. S11. Electron diffraction patterns for HEB. Taken along the zone axes of (a) [21-1] and (b) [-211].

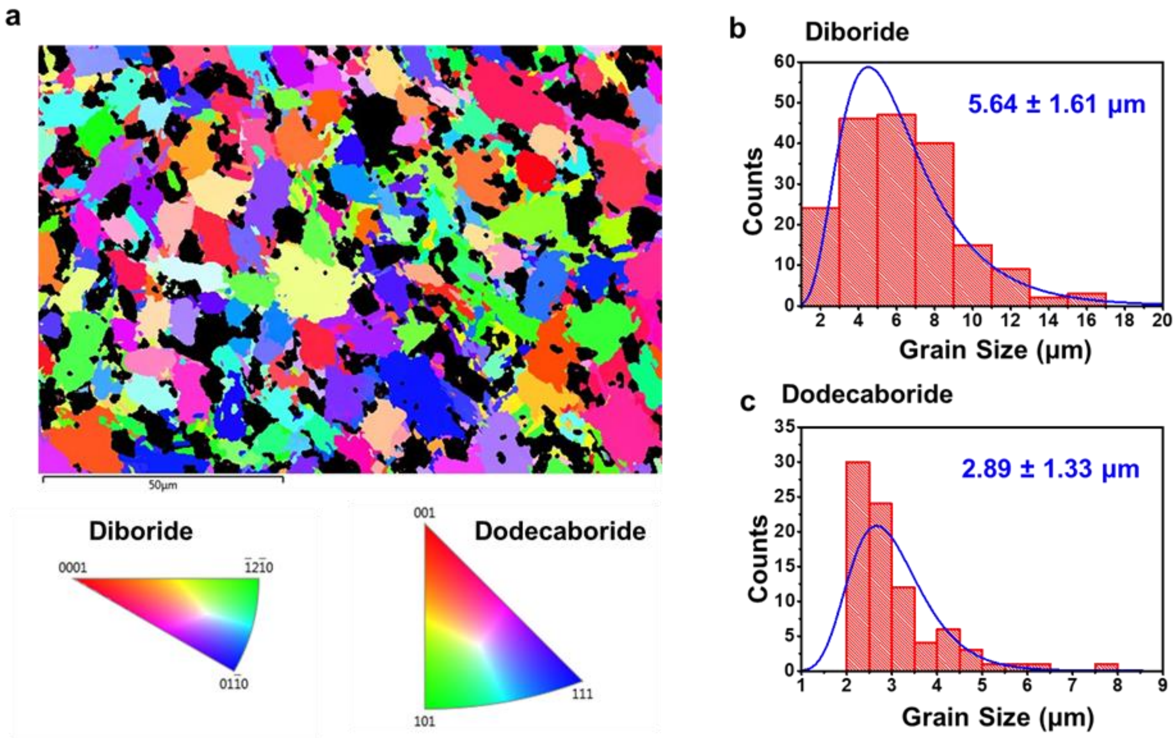

Fig. S12. EBSD analysis reveals the grain size distributions of the HEB and dodecaboride phases. (a) The EBSD normal direction inverse pole figure orientation maps. The grain size distributions of (b) HEB and (c) dodecaboride phases.

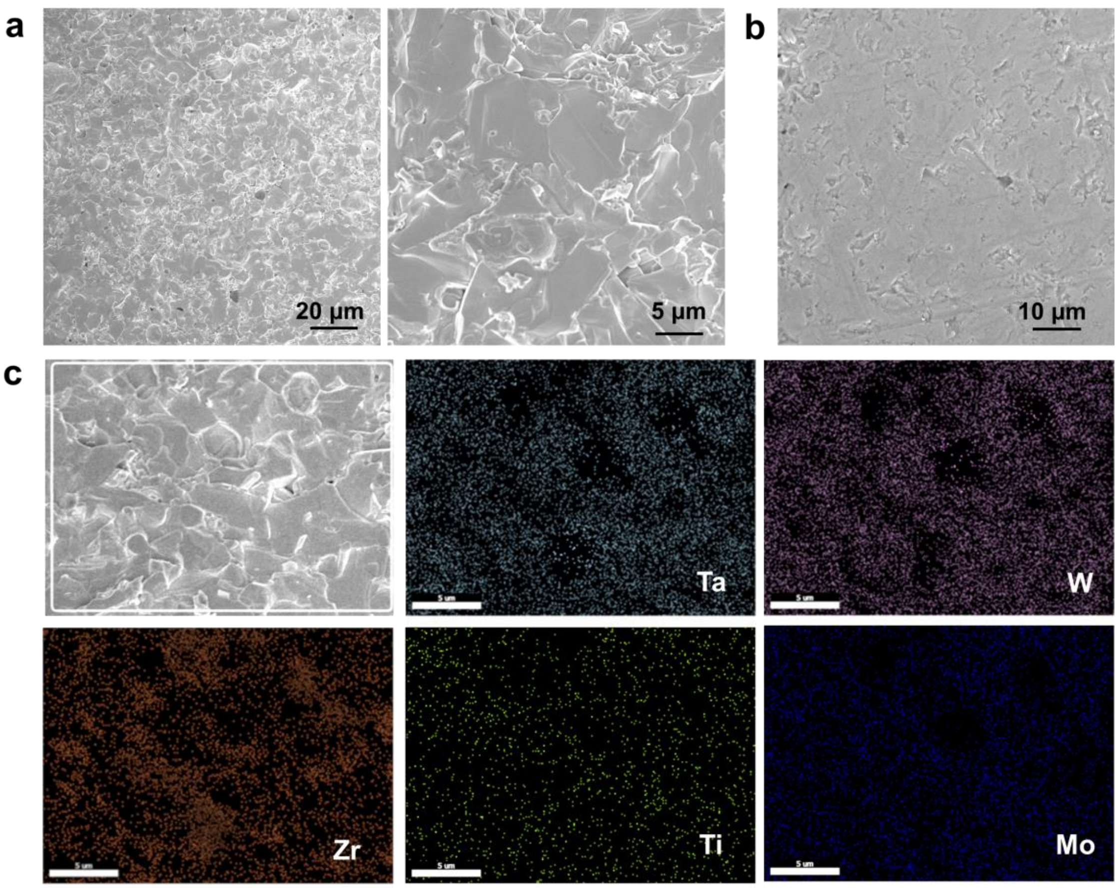

Fig. S13. Morphology and composition analysis of the HEB sample without the boron carbide and dodecaboride phases. (a) The SEM images of the cracked cross-section morphology of the HEB without the boron carbide and dodecaboride phases. (b) The polished cross-section SEM image of the HEB without the boron carbide and dodecaboride phases. (c) EDS mapping of the elemental distribution in the HEB. Compared to the HEB composite sample, the SEM images of the HEB sample without the boron carbide and dodecaboride phases do not show any obvious bright and dark contrast since there is only one diboride phase. Additionally, the sintering result is not as good as the liquid-assisted composite sample as many small pores can be observed.